Highly efficient spatiotemporal coherent control in nanoplasmonics on a nanometer-femtosecond scale by time reversal

Xiangting Li[1,2,*] and Mark I. Stockman[1,†]
[1]*Department of Physics and Astronomy, Georgia State University, Atlanta, Georgia 30303, USA*
[2]*Department of Physics, Shanghai Jiaotong University, Shanghai, 200240, China*
(Received 19 February 2008; revised manuscript received 18 April 2008; published 14 May 2008)

One of the main problems in nanoplasmonics is the active dynamic control of optical local fields. We propose an efficient method to solve this problem. It allows one to impose coherent control of the spatiotemporal localization of the optical excitation energy in nanoplasmonic systems on the nanometer spatial and femtosecond temporal scales. This approach is based on a general idea of time reversal where the nanosystem itself plays the role of an optical antenna and resonator. It is wireless and noninvasive. This method will open up many more fundamental and engineering applications of nanoplasmonics, in particular, to ultrafast computations and information storage on the nanoscale and ultrafast nanoscale spectroscopy.

DOI: 10.1103/PhysRevB.77.195109 PACS number(s): 78.67.−n, 71.45.Gm, 42.65.Re, 73.20.Mf

I. INTRODUCTION

Nano-optics and nanoplasmonics are experiencing presently a period of explosive growth and attracting a great interest. Nanoplasmonics deals with electronic processes at the surfaces of metal nanostructures, which are due to electronic excitations called surface plasmons (SPs), which can localize optical energy on the nanoscale.[1–3] The nanoplasmonic processes can potentially be the fastest in optics: their shortest evolution times are defined by the inverse spectral width of the region of the plasmonic resonances and are on the order of 100 as.[4] The relaxation times of the SP excitations are also ultrashort, in the 10–100-fs range.[5–9] Such nanolocalization and ultrafast kinetics make plasmonic nanostructures promising for various applications, especially for ultrafast computations and data control and storage on the nanoscale.

These and potentially many other applications require precise control over the optical excitations of nanostructures in time and space on the femtosecond-nanometer scale. Such control cannot be imposed by far-field focusing of the optical radiation because the diffraction limits its dimension to greater than half of a wavelength. In other words, optical radiation does not have spatial degrees of freedom on the nanoscale. There is a different class of approaches to control a system on the nanoscale based on plasmonic nanoparticles or waveguides brought to the *near-field* region of the system. Among these we mention the tips of scanning near-field optical microscopes,[1] adiabatic plasmonic waveguides,[10] nanowires,[11,12] plasmonic superlenses,[13] or hyperlenses.[14] In all these cases, a massive amount of metal is brought to the vicinity of the plasmonic nanosystem, which will produce strong perturbations of its spectrum and SP eigenmodes, cause additional optical losses, and adversely affect the ultrafast dynamics and energy nanolocalization in the system. This nanowaveguide approach also may not work because of the excitation delocalization due to the strong interaction (capacitive coupling) at nanoscale distances for optical frequencies.

We have proposed[15] a principally different approach to ultrafast optical control on the nanoscale based on the general idea of coherent control. Coherent control of the quantum state of atoms and molecules is based on the directed interference of the different quantum pathways of the optical excitation,[16–25] which is carried out by properly defining the phases of the corresponding excitation waves. This coherent control can also be imposed by an appropriate phase modulation of the excitation ultrashort (femtosecond) pulse.[22,26–28] Shaping the polarization of a femtosecond pulse has proven to be a useful tool in controlling quantum systems.[29]

Our initial idea[15] has been subsequently developed theoretically[29–32] and confirmed experimentally.[33–35] In this coherent-control approach, one sends from the far-field zone a shaped pulse (generally, modulated by phase, amplitude, and polarization) that excites a wideband packet of SP excitations in the entire nanosystem. The phases, amplitudes, and polarizations of these modes are forced by this shaped excitation pulse in such a manner that at the required moment of time and at the targeted nanosite, these mode oscillations add in phase while at the other sites and different moments of time they interfere destructively, which brings about the desired spatiotemporal localization. Theoretically, the number of effective degrees of freedom that a shaped femtosecond pulse may apply to a nanoplasmonic system is on the order of its quality factor Q (i.e., the number of coherent plasmonic oscillations that system undergoes before dephasing). In the optical region for noble metals, $Q \sim 100$, providing a rich, ~ 100-dimensional space of controlling parameters. The coherent control approach is noninvasive: in principle, it does not perturb or change the nanosystem's material structure in any way.

However, how to actually determine a shaped femtosecond pulse that compels the optical fields in the nanosystem to localize at a targeted nanosite at the required femtosecond time interval is a formidable problem to which until now there has been no general and effective approach. To compare, our initial chirped pulses possessed only two effective degrees of freedom (carrier frequency ω_0 and chirp), which allowed one to concentrate optical energy at the tip of a V-shaped structure versus its opening.[15,30] Similarly, the two unmodulated pulses with the regulated delay τ between them used in the interferometric coherent control[31,33,35] also pos-

sess only two degrees of freedom (τ and ω_0) and can only select one of any two local-field hot spots against the other; it is impossible, in particular, to select one desired hot spot against *several* others.

There exists another method based on adaptive genetic algorithms.[22] However, its application to the spatiotemporal localization in a nanosystem is very difficult due to the complexity of the problem. To date, the only example is the spatial concentration of the excitation on one arm of a three-pronged metal nanostar[34] where the obtained controlling pulses are very complicated and difficult to interpret though the nanosystem itself is very simple. A general problem with this method is that the adaptive genetic algorithms are actually refined trial-and-error methods; they do not allow one to obtain the required controlling pulses as a result of the solution of a set of deterministic equations or the application of any regular deterministic procedure such as Green's function integration. Any demonstration of this method for time-space localization or more complicated nanoplasmonic systems has never been carried out.

Our solution of this major problem of coherent control, which is proposed and theoretically developed in this article, is based on an idea of time reversal that has originally been proposed and used to control the focusing of acoustic waves and microwave radiation.[36–38] Some of these studies required use of a reverberating chamber to cause multiple interactions of the waves with the system needed to transfer the information to the far field. The electromagnetic subwavelength focusing also required a subwavelength-scale metal structure (a metal wire brush) to be positioned in the vicinity of the target system as a focusing antenna. In contrast, in nanoplasmonics there is no need for a reverberating chamber or metal brush antenna, because the plasmonic nanosystem plays the roles of both of them. It confines the plasmonic modes for long times relative to their oscillation periods and also nanolocalizes these modes.

II. QUALITATIVE DESCRIPTION

The idea of our time-reversal solution of nanoscale coherent control can be described using the schematic of Fig. 1. Consider a metal plasmonic nanosystem, indicated by blue, which may be embedded in a host dielectric (or be in vacuum). The nanosystem is excited by an external ultrafast (femtosecond) nanosource of radiation at its surface. As such, we choose an oscillating dipole indicated by a double red arrow in panel (a). This dipole generates a local optical electric field shown by a bold red wave form. This field excites SP oscillations of the system in its vicinity; in turn, these oscillations excite other, more distant regions, and so forth until the excitation spreads out over the entire system. The relatively long relaxation time of these SP modes leads to the long "reverberations" of the plasmonic fields and the corresponding far-zone optical electric field. The latter is shown in Fig. 1(b) where one can see that a complicated vector wave form is predicted. This wave form is time reversed, as shown in panel (c), and sent back to the system as an excitation plane wave from the *far* zone. If the entire field, in the whole space including the near-field (evanescent)

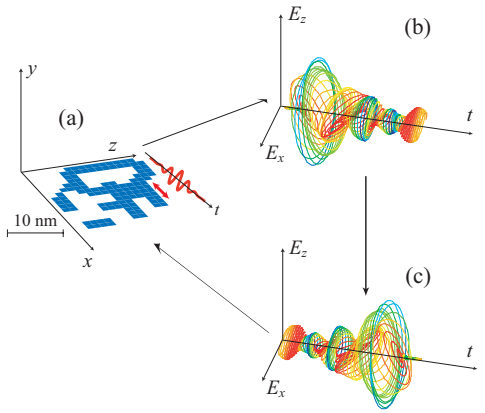

FIG. 1. (Color) (a) Geometry of a nanosystem, initial excitation dipole, and its oscillation wave form. The nanosystem as a thin nanostructured silver film is depicted in blue. A position of the oscillating dipole that initially excites the system is indicated by a double red arrow, and its oscillation in time is shown by a bold red wave form. (b) Field in the far-field zone that is generated by the system following the excitation by the local oscillating dipole: the vector $\{E_x(t), E_z(t)\}$ is shown as a function of the observation time t. The color corresponds to the instantaneous ellipticity as explained in the text in connection with the figure. (c) Same as in panel (b), but for a time-reversed pulse in the far zone that is used as an excitation pulse to drive the optical energy nanolocalization at the position of the initial dipole.

zone, were time reversed *and* the system were completely time reversible, which would imply the absence of any dielectric losses, then the system would have been compelled by this field exactly to back-trace its own evolution in time. This would have led to a concentration of the local optical energy exactly at the position of the initial dipole at a time corresponding to the end of the excitation pulse.

Indeed, the system is somewhat lossy, which means that it is not exactly time reversible. Nevertheless, these losses are small, and one may expect that they will not principally change the behavior of the system. Another problem appears to be more significant: the evanescent fields contain the main information of the nanodistribution of the local fields in the system, and they cannot be time reversed from the far zone because they are exponentially small, practically lost there. However, our idea is that the nanostructured metal system itself plays the role of the metal brush of Ref. 38 continuously coupling the evanescent fields to the far zone. Therefore the fields in the far zone actually contain, in their reverberations, most information about the evanescent fields that will be regenerated in the process of the time reversal. These two arguments, regarding the possibility to neglect the losses and the regeneration of the near fields, of course, should and will be scrutinized and confirmed by our computations presented farther in this article.

III. CALCULATIONS AND RESULTS

A. System and calculations

We will illustrate our idea by considering a random plasmonic nanolayer whose geometry is shown in gray in the

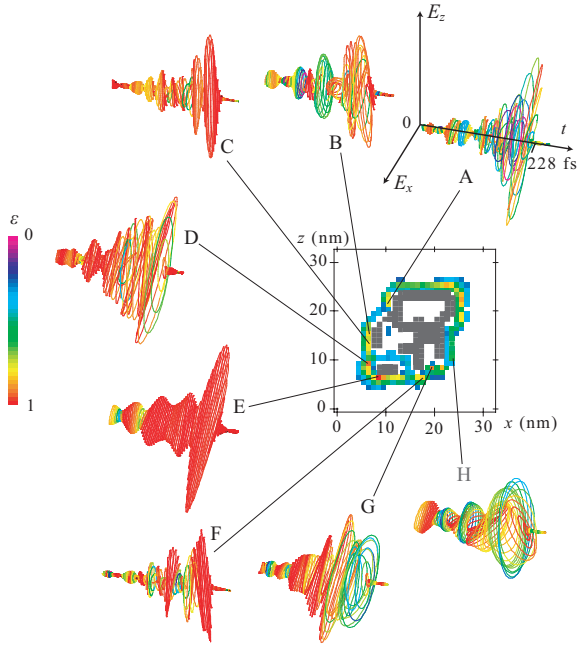

FIG. 2. (Color) Schematic of plasmonic-nanosystem geometry, local fields, and pulses generated in the far field. Central inset: The geometry of a nanosystem is shown by dark gray, and the local fields in the region surrounding it are shown by colors. The highest local field intensity is depicted by red, and the lowest intensity is indicated by blue (in the rainbow sequence of colors). $A-H$: the excitation wave forms in the far fields obtained as described in the text by positioning the initial excitation dipole at the metal surface at the locations indicated by the corresponding lines. Coordinate vectors $\boldsymbol{\rho}$ of points $A-H$ in the xz plane are (in nm) $\boldsymbol{\rho}_A=(11,22)$, $\boldsymbol{\rho}_B=(7,16)$, $\boldsymbol{\rho}_C=(7,14)$, $\boldsymbol{\rho}_D=(7,10)$, $\boldsymbol{\rho}_E=(9,7)$, $\boldsymbol{\rho}_F=(18,7)$, $\boldsymbol{\rho}_G=(20,9)$, and $\boldsymbol{\rho}_H=(24,11)$. The instantaneous degree of linear polarization ε is calculated as the eccentricity of an instantaneous ellipse found from a fit to a curve formed by the vector $\{E_x(t),E_y(t)\}$ during an instantaneous optical period. The pure circular polarization corresponds to $\varepsilon=0$ and is denoted by blue-violet color; the pure linear polarization is for $\varepsilon=1$ indicated by red. The corresponding polarization color-coding bar is shown at the left edge of the figure.

center of Fig. 2. In specific computations, as the plasmonic metal, we consider silver whose dielectric permittivity ε_m we adopt from bulk data.[39] This system has been generated by randomly positioning $2\times2\times2$ nm^3 metal cubes on a plane, which for certainty we will consider as the x-z coordinate plane. The random system shown in the center of Fig. 2 has filling factor of 0.5.

The interaction of a nanosystem with electromagnetic pulses is described by a Green's function approach using a quasistatic approximation[15,30,40]; some necessary details of this approach are given in the Appendix. It is known that the optical excitation energy in random plasmonic nanostructures localizes in "hot spots" whose size is on the nanoscale and is determined by the minimum scale of the system inhomogeneities.[3,41,42] Initially, to find positions of these hot spots in our system, we apply an ultrashort near-infrared (near-ir) pulse whose spectral width was very large, covering a band from 1.1 eV to 1.7 eV. The pulse polarization is along the z axis (the incidence direction is normal to the plane of the nanostructure—i.e., along the y axis). The resulting optical electric field $\mathbf{E}$ is expressed in terms of the external electric field of the excitation optical wave $\mathbf{E}_0$ and retarded dyadic Green's function $\mathbf{G}^r$,

$$\mathbf{E}(\mathbf{r},t)=\mathbf{E}_0(\mathbf{r},t)+\int d^3r'\ dt'\ \mathbf{G}^r(\mathbf{r},\mathbf{r}';t-t')\Theta(\mathbf{r}')\mathbf{E}_0(t'), \tag{1}$$

where the Θ function is unity within the metal component and zero in the surrounding dielectric; the integration over coordinates $\mathbf{r}'$ is extended over the entire volume of the system, and the integration over time t' is running over the duration of the excitation pulse. Green's functions, which enter here and below in this paper, are expressed and some details of the techniques are presented in the Appendix.

The hot spots are always localized at the surface of the metal, predominantly at the periphery of the system. Their intensities found as the result of these computations are depicted by colors in the center of Fig. 2. The highest local intensity is indicated by red and the lowest by blue in the region surrounding the metal. We have selected eight of these hot spots for our computations as denoted by letters $A-H$ in the figure.

To generate the field in the far zone, we take a point dipole and position it at a surface of the metal at point $\mathbf{r}_0$ at such a hot spot, as described in the discussion of Fig. 1 above. The near-zone field $\mathbf{E}^L(\mathbf{r},t)$ generated in response to this point dipole is found from Green's function relation (see the Appendix)

$$\mathbf{E}^L(\mathbf{r},t)=\frac{4\pi}{\varepsilon_d}\int dt'\ \mathbf{G}^r(\mathbf{r},\mathbf{r}_0;t-t')\mathbf{d}(\mathbf{r}_0,t'), \tag{2}$$

where ε_d is the permittivity of the surrounding dielectric.

Knowing this local electric field, we calculate the total radiating optical dipole moment of the nanosystem in the frequency domain as

$$\mathbf{D}(\omega)=\frac{1}{4\pi}\int d^3r[\varepsilon_m(\omega)-\varepsilon_d]\Theta(\mathbf{r})\mathbf{E}^L(\mathbf{r},\omega). \tag{3}$$

Here and below, the frequency- and time-domain quantities, as indicated by their arguments ω and t, are Fourier transforms of each other. The field in the far zone produced by this radiating dipole is given by standard electrodynamic formula (see, e.g., Sec. 67 in Ref. 43). The time-reversed field is generated by the time-reversed dipole $\mathbf{D}^T(t)$, which is complex conjugated in the frequency domain, $\mathbf{D}^T(\omega)=\mathbf{D}(\omega)^*$.

The dependence on time of the initial excitation dipole, $\mathbf{d}(\mathbf{r}_0,t)$, was an ultrashort Gaussian-shaped pulse of 12 fs duration with the carrier frequency $\hbar\omega_0=1.2$ eV. Following the procedure described above, the fields shown in Figs. 1 and 2 have been calculated for the radiation propagating in the y direction (normal to the plane of the nanostructure). These fields simply copy the retarded time evolution of the emitting dipole.

At the completing stage of our calculations, the time-reversed excitation pulse is sent back to the system as a plane wave propagating along the y direction (normal to the nanosystem plane). To calculate the resulting local fields, we again use Green's function (1) where the shaped excitation pulse substitutes for field $\mathbf{E}_0$.

B. Excitation pulses

The electric field of the excitation wave was a modulated wave form (including amplitude, phase, and polarization modulation) that has been computed as described above in the previous subsection. The optical excitation energy can only be concentrated at sites where SP eigenmodes localize. For the present system, these are the hot spots shown by color in the central insert of Fig. 2, labeled $A-H$. The corresponding calculated excitation wave forms are displayed in panels as vector plots shown as functions of time $\{E_x(t), E_z(t)\}$.

There are several important features of these wave forms deserving our attention and discussion. First, these wave forms are rather long in duration: much longer than the excitation-dipole 12-fs pulses. This confirms our understanding that the initial dipole field excites local SP fields that, in a cascade manner, excite a sequence of the system SPs, which ring down relatively long time (over 200 fs, as shown in the figure). This long ring-down process is exactly what is required for the nanostructure to transfer to the far-field zone the information on the near-zone local (evanescent) fields as is suggested by our idea presented above in the Introduction. The obtained fields are by shape very similar to the controlling pulses for the microwave radiation.[38] However, a principal difference is that in the microwave case the long ringing-down is due to the external reverberation chamber, while for the nanoplasmonic systems it is due to the intrinsic evolution of the highly resonant SP eigenmodes that possess high-Q factors (setting a reverberation chamber around a nanosystem would have been, indeed, unrealistic).

Second, one can see that the pulses in Fig. 2 have a very nontrivial polarization properties ranging from the pure linear polarization (indicated by red as explained in the caption to Fig. 2) to the circular polarization indicated by blue, including all intermediate degrees of circularity. The temporal-polarization structure of pulses $A-H$ in Fig. 2 is very complicated, somewhat recalling that of Ref. 34, which was obtained by a genetic adaptive algorithm. However, in our case these pulses are obtained in a straightforward manner by applying the well-known deterministic Green's function of the system, which is a highly efficient and fast method.

The third, and most important, feature of the wave forms in Fig. 2 is that they are highly site specific: pulses generated by the initial dipole in different positions are completely different. This is a very strong indication that they do transfer to the far-field zone the information about the complicated spatiotemporal structure of the local near-zone fields. This creates a prerequisite for studying the possibility of using these pulses for coherently controlled nanotargeting.

C. Controlled nanofocusing: Calculation results

Now we turn to the crucial test of the nanofocusing induced by the excitation pulses discussed above in conjunction with Fig. 2. Because of the finite time window ($T=228$ fs) used for the time reversal, all these excitation pulses end and should cause the concentration of the optical energy (at the corresponding sites) at the same time, $t=T=228$ fs (counted from the moment the excitation pulse starts impinging on the system). After this concentration instant, the nanofocused fields can, in principle, disappear (dephase) during a very short period on the order of the initial dipole pulse length—i.e., ~ 12 fs. Thus this nanofocusing is a dynamic, transient phenomenon.

Note that averaging (or integration) of the local-field intensity $I(\mathbf{r},t)=|\mathbf{E}(\mathbf{r},t)|^2$ over time t would lead to the loss of the effects of the phase modulation. This is due to a mathematical equality $\int_{-\infty}^{\infty} I(\mathbf{r},t)dt=\int_{-\infty}^{\infty}|\mathbf{E}(\mathbf{r},\omega)|^2 d\omega/(2\pi)$, where the phase of the field is certainly eliminated from the expression on the right-hand side. Thus the averaged intensity of the local fields is determined only by the local power spectrum of the excitation $|\mathbf{E}(\mathbf{r},\omega)|^2$ and, consequently, is not coherently controllable. Very importantly, such a cancellation is not valid for nonlinear phenomena. In particular, two-photon processes such as two-photon fluorescence or two-photon electron emission, which can be considered as proportional to the squared intensity $I^2(\mathbf{r},t)=|\mathbf{E}(\mathbf{r},t)|^4$, are coherently controllable even after time averaging (integration), as we have argued earlier.[30,31] Note the distributions measured in nonlinear optical experiments with the detection by the photoemission electron microscope[33–35,44] (PEEM) and in the fluorescence up-conversion experiments[45] can be modeled as such nonlinear processes that yield the distributions $\langle I^n(\mathbf{r})\rangle=\int_{-\infty}^{\infty} I^n(\mathbf{r},t)dt/T$, where $n\geq 2$. Inspired by this, we will also consider below the coherent control of the two-photon process average intensity $\langle I^2(\mathbf{r})\rangle$.

To establish the controlled nanofocusing and elucidate the role of the polarization pulse shaping, we start by comparing two pulses E and H. As we see from Fig. 2, pulse E is almost purely linearly polarized, while pulse H shows a high degree of circular polarization during a period close to its maximum amplitude. The results of computations using these two pulses are shown in Fig. 3. Note that the excitation pulses used in the computations have not been specially normalized. Thus only the distribution of the intensities is meaningful, but not their absolute magnitude, which depends on the arbitrary excitation pulse power.

For the excitation with pulse E, the resulting distributions over the surface of the metal nanostructure are displayed in Figs. 3(a)–3(d). First, we use only the x-polarized component of the excitation pulse. The result shown in panel (a) shows a pronounced concentration of the averaged two-photon excitation distribution $\langle I^2(\mathbf{r})\rangle$ at the targeted E site. Equally excellent targeted localization takes place with the z-polarized component [panel (b)]. The use of the full polarization-shaped pulse [panel (c)] yields a similar result. This shows an excellent coherent controllability of the optical energy localization at this site and also the absence of a significant effect of the polarization pulse shaping in this case. The dynamic localization of the local field intensity $I(\mathbf{r},t)$ is shown in Fig. 3(d) at the target time of $t=228$ fs for the full shaped pulse; this localization is also excellent. The fact that a single polarization is sufficient in this to localize the excitation at the target side is certainly related to the fact

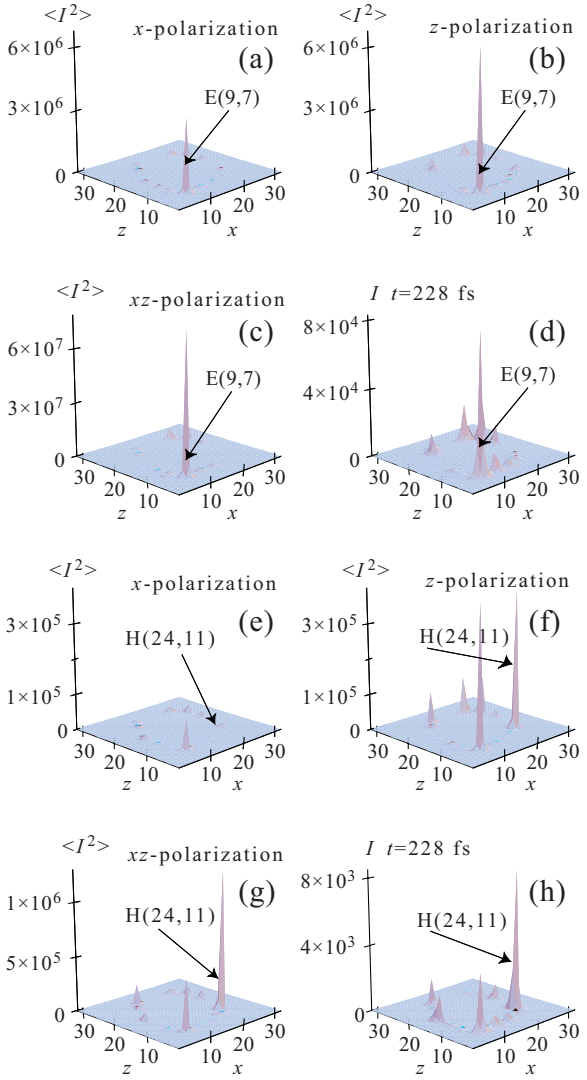

FIG. 3. (Color online) Spatial distributions of optical excitation at the surface of the nanosystem. These distributions are not normalized in any special way, so that only the distribution form within one panel is informative; the relative magnitudes between the panels depend on the intensity of the excitation and are arbitrary. (a) Distribution of averaged two-photon excitation rate $\langle I^2(\mathbf{r})\rangle$ for the linear x-polarization of the excitation pulse E. (b) The same as panel (a), but for the linear z-polarization. (c) The two-photon distribution $\langle I^2(\mathbf{r})\rangle$ for the full polarization shaped (xz polarization) excitation pulse E. (d) The same as panel (c), but for the distribution of the instantaneous local field intensity $I(t)$ for the instance $t=228$ fs when the intensity at the targeted site reaches its maximum. (e)–(h) The same as panels (a)–(d), but for the excitation pulse H.

that the far-zone pulse generated by the local-dipole excitation procedure is almost completely linearly polarized—cf. Fig. 2, pulse E.

In sharp contrast, pulse H contains a significant degree of circular polarization; cf. Fig. 2. The corresponding distributions of the averaged two-photon excitation, $\langle I^2(\mathbf{r})\rangle$, are shown in Figs. 3(e)–3(g). It is obvious that any single linear polarization is not efficient: for the x polarization there is no appreciable concentration at the targeted site [panel (e)], and for the z polarization the distribution weight is almost evenly split between the targeted site and another one. It is remarkable that the full polarization pulse induces a very good concentration of the distribution $\langle I^2(\mathbf{r})\rangle$ at targeted site H; see panel (g). The temporal dependence of the distribution shows that at the expected time $t=228$ fs the optical energy is sharply peaked at the targeted site H [panel (h)]. Thus, inclusion of the polarization in the control parameters in this case is both necessary and efficient.

Now we investigate how precisely one can achieve the spatiotemporal focusing of the optical excitation at a given nanosite of a plasmonic nanostructure using the full shaping (amplitude, phase, and polarization) of the excitation pulses found from the time-reversal method. The results for the present nanostructure, targeting sites $A-H$, are shown in Fig. 4. For each excitation pulse, the spatial distribution of the local field intensity is displayed for the moment of time when this local intensity acquires its global (highest) maximum. The most important conclusion that one can draw from comparing panels (a)–(f) is that for each pulse $A-H$ this global maximum corresponds to the maximum concentration of the optical energy at the corresponding targeted nanosite $A-H$. This obtained spatial resolution is as good as 4 nm, which is determined by the spatial size of inhomogeneities of the underlying plasmonic metal nanosystem. It is very important that this localization occurs not only at the desired nanometer-scale location, but also very close to the targeted time, which in our case is $t=228$ fs. Thus the full shaping of femtosecond pulses by time reversal is an efficient method of controlling the spatiotemporal localization of energy at the femtosecond-nanometer scale.

Let us turn to the temporal dynamics of intensity of the nanoscale local fields at the targeted sites $A-H$, which is shown in Figs. 5(a)–5(h). As we can see, in each of the panels there is a sharp spike of the local fields very close to the target time of $t=228$. The duration of this spike in most panels [(a)–(f)] is close to that of the initial dipole—i.e., 12 fs. This shows a trend to the reproduction of the initial excitation state due to the evolution of the time-reversed SP packet induced by the shaped pulses. There is also a pedestal that shows that this reproduction is not precise, which is expected due to the fact that the time reversal is incomplete: only the far-zone field propagating in one direction (along the y axis) is reversed. Nevertheless, as the discussion of Fig. 4 shows, this initial excitation-state reproduction is sufficient to guarantee that the targeted (initial excitation) site develops the global maximum (in time and space) of the local-field intensity. Interesting enough, the trend to reproduce the initial excitation state is also witnessed by almost symmetric (with respect to the maximum points $t=228$ fs) shapes of all wave forms, which occurs in spite of the very asymmetric shapes of the excitation wave forms (cf. Fig. 2).

Apart from the ultrafast (femtosecond) dynamics of the nanolocalized optical fields discussed above in conjunction with Figs. 4 and 5, there is a great interest in its the time-integrated or averaged distributions—in particular, the mean-squared intensity $\langle I^2(\mathbf{r})\rangle$. This quantity defines the nanoscale spatial distribution of the incoherent two-photon processes. In some approximation, the spatial distribution of the two-photon electron emission recorded by PEEM,[33–35,44] as we have already indicated discussing Fig. 3, is determined by $\langle I^2(\mathbf{r})\rangle$.

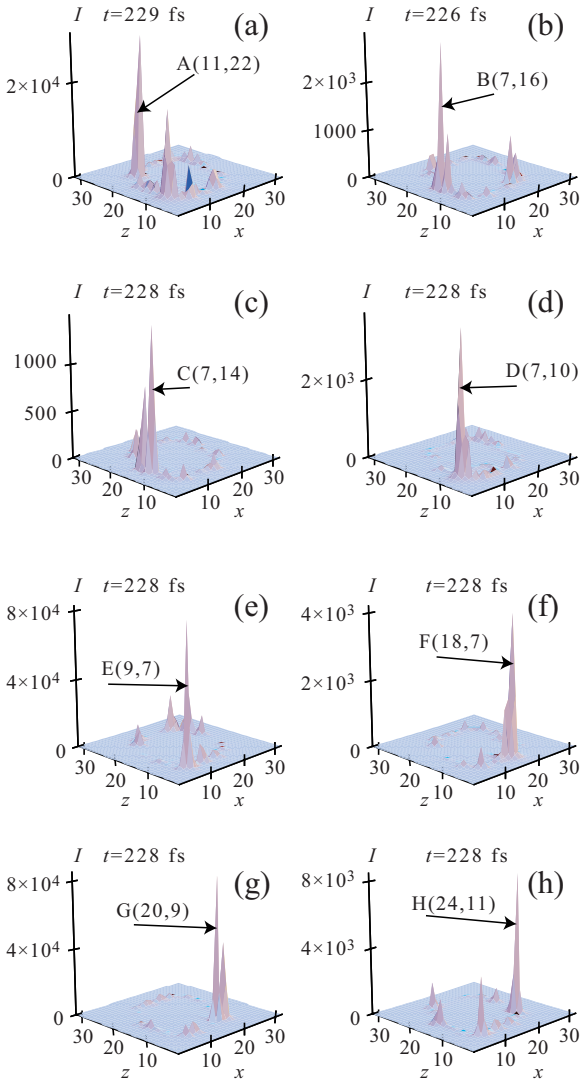

FIG. 4. (Color online) Spatial distributions of the local optical field intensities at the surface of the metal nanostructure. Panels (a)–(h) correspond to the excitation with pulses $A-H$. Each such a distribution is displayed for the instance t at which the intensity for a given panel reaches its global maximum in space and time. This time t is displayed at the top of the corresponding panels. The corresponding targeted sites are indicated by arrows and labeled by the corresponding letters $A-H$ and the coordinates (x,z). No special normalization has been applied so the distribution within any given panel is informative, but not necessarily the magnitudes of the intensities between the panels. Panels (e) and (h), which were already shown in Fig. 3 as panels (d) and (h), are given also here for the sake of completeness and convenience.

We have already shown above, in conjunction with Fig. 3, that there is a spatial concentration of the averaged mean-squared intensity $\langle I^2(\mathbf{r})\rangle$ for sites E and H. In Fig. 6, we test such concentration for all sites (including the E and H sites for the sake of completeness). As clearly follows from this figure, in all cases, there are leading peaks at the targeted sites. Thus the two-photon excitation, even after the time averaging, can be concentrated at desired sites using the coherent-control by the time-reversed shaped pulses.

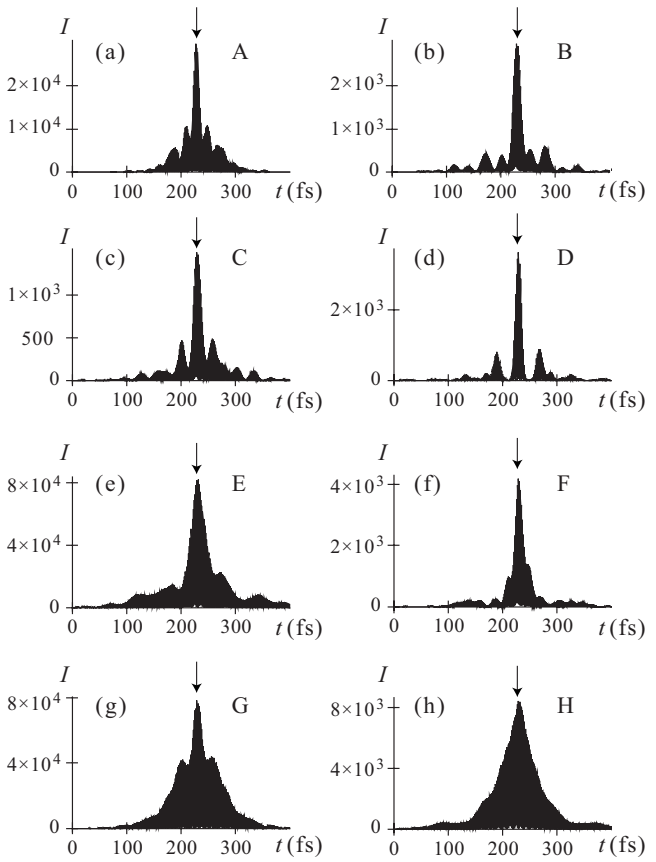

FIG. 5. (a)–(h) Temporal dynamics of the local field Intensity $I(\mathbf{r},t)=\mathbf{E}^2(\mathbf{r},t)$ at the corresponding hot spots $A-H$. The down-arrows mark the target time $t=228$ fs where the local energy concentration is expected to occur.

IV. DISCUSSION AND CONCLUSIONS

The spatiotemporal control of the optical excitation of a nanosystem on a nanometer-femtosecond scale is one of the most important and fundamental problems of nanoplasmonics and nanotechnology. In the conventional microelectronics, this problem is solved using metal (currently, copper) wire interconnects. However, for optical frequencies and nanometer spatial dimensions, this approach cannot work because of the excitation delocalization due to the strong interaction at the nanoscale distances. We have proposed a principally different approach to this formidable problem that is based on the idea of coherent control that is a directed interference between system's eigenmodes.[15] In this approach, one does not attempt a localized excitation of a plasmonic nanosystem: generally, such an excitation will delocalize over the entire system during femtosecond time intervals. To the opposite, one excites a wideband packet of SP excitations in the entire system. The phases, amplitudes, and polarizations of these modes are forced by the excitation pulse in such a way that at the required moment of time and at the targeted nanosite, these mode oscillations add in phase while at the other sites and different moments of time they interfere destructively.

This idea allows a targeted ultrafast (femtosecond-scale) and localized (nanometer-scale) excitation, but is completely

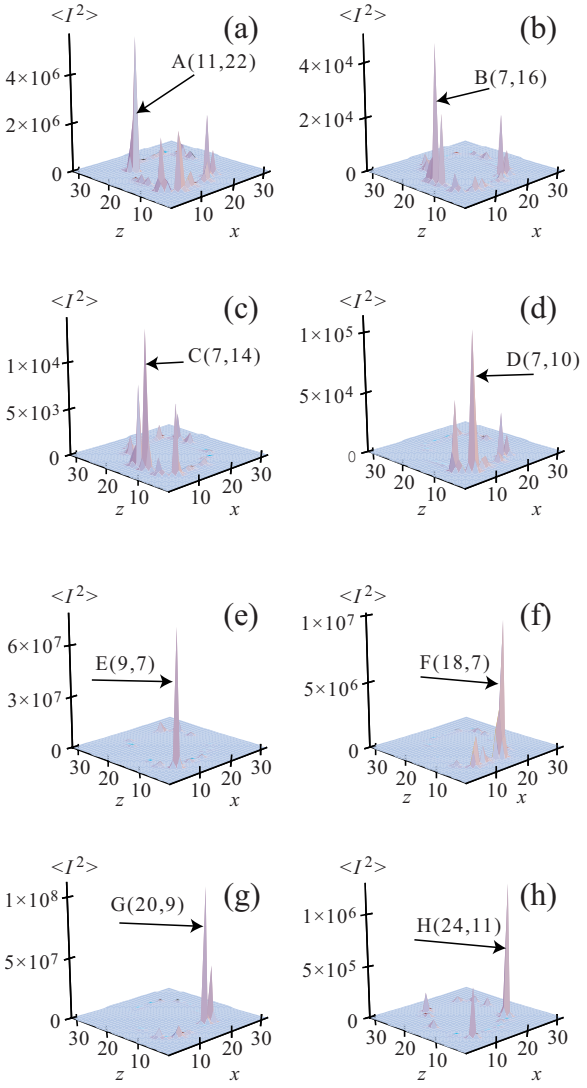

FIG. 6. (Color online) Spatial distributions of the time-averaged mean-squared intensity $\langle I^2(\mathbf{r})\rangle$. This represents, in particular, the spatial distribution of the two-photon excited photocurrent density. Panels (a)–(h) correspond to the excitation with pulses $A-H$. The corresponding targeted sites are indicated by arrows and labeled by the corresponding letters $A-H$ and coordinates (x,z). No special normalization has been applied so the distribution within any given panel is informative, but not necessarily the magnitudes of the intensities between the panels. Panels (e) and (h), which were already shown in Fig. 3 as panels (c) and (g), are given also here for the sake of completeness and convenience.

dependent on the possibility to find the corresponding controlling pulse that is, in a general case, fully modulated by amplitude, phase, and polarization. Finding such a pulse for a specific location in a nanosystem is a formidable problem that, in principle, could be solved by using adaptive algorithms.[22,23] However, the solutions obtained by this method can be very complicated even for simple systems[34] and are difficult to interpret. There were no examples or approaches to the full spatiotemporal control of complex nanoplasmonic systems.

In this article we propose and develop a principally different approach based on the idea of time reversal. Nanoplasmonic systems of noble metals in the optical range of frequencies have high resonant quality (low losses) and therefore, in principle, are almost time reversible. However, a significant problem is that the evanescent (near-zone) fields are vanishingly (exponentially) small in the far zone and therefore cannot be reversed.

Our present idea is that a plasmonic nanosystem, due to its high resonant quality, traps and sustains the optical oscillations for a relatively long time (~100 fs). The oscillating optical fields continuously interact with the plasmonic nanostructure, transferring the information from the evanescent (near-zone) fields to radiative (far-zone) fields where it is encoded into the field temporal dynamics. A direct piece of evidence of such a transfer is illustrated in Fig. 2 where the wave forms emitted by the locally excited nanosystem are long, ringing down for many oscillation periods, and are *highly specific* for the position of the initial excitation.

This time-reversal approach can, in principle, be implemented not only theoretically, but also experimentally, by positioning a fluorescent emitter (for example, a semiconductor nanocrystal quantum dot) at the desired site of the nanosystem and exciting it externally with an optical pulse in the ultraviolet spectral range that does not by itself cause a resonant response of the nanosystem. Such quantum dots are photochemically stable emitters, and accumulating statistics over many pulses one can find the field of the pulse in the far zone. The required time reversal can then be effected using the standard pulse-shaping techniques.

The present theory allows one to determine the required controlling pulses (wave forms) without the cumbersome and time-consuming adaptive algorithms by a direct integration with Green's function—see Eq. (2). Green's function can be found as a solution of a relatively simple, deterministic boundary problem, which is outlined in the Appendix, by standard numerical grid or multipole methods. This is how the controlling pulses shown in Fig. 2 have been computed. These pulses carry full modulation (shaping): amplitude, phase, and polarization. Among them, the polarization shaping is important in many cases as Fig. 3 demonstrates.

These pulses have proved to be very efficient in the spatial concentration of the local optical-field energy at the targeted sites at the desired moments of time, as the results shown in Fig. 4 demonstrate. This concentration occurs not only in space, but also in time, tending to reproduce the ultrashort pulse of the seed dipole—see Fig. 5.

For nonlinear effects, in particular two-photon excitation, the concentration at the targeted site occurs not only at a chosen time, but also on average during the entire time—see Fig. 6. This opens up a possibility to coherently control and study the local optical energy nanoconcentration with time-integrating inertial devices such as PEEM in Refs. 33–35. In the case of multiphoton excitation, in particular the nonlinear electron emission for relatively low (infrared) excitation frequencies or cascade upconversion,[45] such a time-averaged concentration will be even more pronounced.

It is also fundamentally important to understand why it is possible to control so well such a complicated system as metal plasmonic nanostructure whose eigenmodes not only tend to delocalize over the entire system,[3,41] which occurs due to the long-range dipole interaction,[46] but also are

chaotic.[42] The fundamental reason is that, similar to quantum-mechanical chaos, the plasmonic systems under consideration possess a discrete spectrum of SP eigenmodes.[3] Such systems with the discrete spectra can exhibit quasirandom chaotic behavior properties, but still are well time reversible.

Our method allows for precise control of the nanosystems by far-zone fields without any metal wires connecting them to the external world. This is of paramount importance for future applications of nanoplasmonics. The metal connectors would bring many serious drawbacks to the optical-frequency nanoscale devices: they are too slow, cross talking due to the surrounding fields, and perturbing (in particular, metal wires close to the nanoplasmonic circuitry cause dielectric losses).

The proposed method of time-reversal coherent control is efficient and noninvasive: this control is carried out from the far zone using the nanoplasmonic system itself as an optical nanoantenna without any additional metal parts. Another potential approach of the coupling nanosystems to the far-zone fields can consist in the use of the so called magnifying superlenses ("perfect lenses"),[13] hyperlenses,[14] or adiabatic concentrators[10] including those based on metal-wire arrays.[11,12] In all these cases, a massive amount of metal should be brought to the vicinity of the plasmonic nanosystem, which will cause correspondingly massive perturbations of the spectrum and SP eigenmodes, losses, etc. With respect to all these methods, which together can be called nanowaveguide approaches, our proposed time-reversal coherent control has great potential advantages of being noninvasive, fast, and having a high spatial resolution on the nanoscale, unattainable by other approaches.

Our proposed time-reversal method is also remarkably stable computationally, as one can see from the results of Sec. III C. This is clear already from the fact that the very precise concentration of optical energy at a given site and time is achieved using only very small part of the information contained in the problem: only the far-zone field is used at a single spatial point. The near-zone fields, which contain the most information, are not used at all, in accordance with the physical problem of far-field control. Another direct piece of evidence of the numerical stability stems from the fact that all the computations have been done with single precision and a relatively small number of harmonics (128–1024) employed in the determination of the temporal dependences. The grid of the system is also not extremely fine (1–2 nm) compared to the obtained spatial resolution of 4 nm. All this allows one to expect that this method will also be stable under experimental conditions.

Now let us discuss potential applications of the targeted excitation of a nanosystem with shaped optical pulses, which may be many. One of the first and, potentially most important, applications is that to the ultrafast (with frequencies from terahertz to optical) computations on the nanoscale. As follows from the results presented above in Sec. III C, it is possible to supply optical energy (which can be transformed on-site into the electrical energy using optical rectification) and controlling pulses to plasmonic nanocircuits or electronic nanochips with optical plasmonic antennas. Another class of applications are in time-resolved local spectroscopy with nanoscale resolution, or directed photochemistry on the nanoscale. Related are applications to optical recording and retrieval of information with nanoscale density of bits. Yet another application may be the creation of nanoscale sources of ultrashort electron-beam pulses, which can find their own applications in the future. Many other potential applications may be possible that are hard even to foresee at this time.

ACKNOWLEDGMENTS

This work was supported by grants from the Chemical Sciences, Biosciences and Geosciences Division of the Office of Basic Energy Sciences, Office of Science, (U.S.) Department of Energy, NSF Grant No. CHE-0507147, and a grant from the U.S.-Israel BSF.

APPENDIX: METHOD

In this appendix, for the sake of completeness and convenience, we outline obtaining Green's function expressions within the framework of spectral theory.[3,30,40] Consider a system consisting of a metal with dielectric permittivity $\varepsilon(\omega)$ embedded in a dielectric background with dielectric constant ε_d. The geometry of the system is described by the characteristic function $\Theta(\mathbf{r})$, which equals 1 in the metal and 0 in the dielectric.

For a nanosystem, which has all sizes much less than the relevant electrodynamic dimensions (radiation wavelength across the propagation direction of the excitation wave and the skin depth in this direction), the quasistatic approximation is applicable. In such a case, we can take into account only static optical potential $\varphi(\mathbf{r},t)$. In the frequency domain, it satisfies the continuity equation

$$\left[\frac{\partial}{\partial \mathbf{r}}\Theta(\mathbf{r})\frac{\partial}{\partial \mathbf{r}} - s(\omega)\frac{\partial^2}{\partial \mathbf{r}^2}\right]\varphi(\mathbf{r},\omega) = 0, \tag{A1}$$

where $s(\omega)=[1-\varepsilon_m(\omega)/\varepsilon_d]^{-1}$ is the spectral parameter.[47] Here φ satisfies the Dirichlet condition at the boundary of the system, $\varphi(\mathbf{r},\omega)=\varphi_0(\mathbf{r},\omega)$, where $\varphi_0(\mathbf{r},\omega)$ is the external (excitation) electric field potential.

The Green's function satisfies a similar equation with the δ-function right-hand side

$$\left[\frac{\partial}{\partial \mathbf{r}}\Theta(\mathbf{r})\frac{\partial}{\partial \mathbf{r}} - s(\omega)\frac{\partial^2}{\partial \mathbf{r}^2}\right]\bar{G}^r(\mathbf{r},\mathbf{r}';\omega) = \delta(\mathbf{r}-\mathbf{r}') \tag{A2}$$

and homogeneous Dirichlet boundary conditions $\bar{G}^r(\mathbf{r},\mathbf{r}';\omega)=0$ for $\mathbf{r}$ (or $\mathbf{r}'$) on the boundary.

It is convenient to expand the Green's function over eigenmodes $\varphi_n(\mathbf{r})$ and the corresponding eigenvalues s_n that satisfy a homogeneous counterpart of Eq. (A1):

$$\left[\frac{\partial}{\partial \mathbf{r}}\Theta(\mathbf{r})\frac{\partial}{\partial \mathbf{r}} - s_n\frac{\partial^2}{\partial \mathbf{r}^2}\right]\varphi_n(\mathbf{r}) = 0, \tag{A3}$$

where $\varphi_n=0$ at the boundary. This spectral expansion of the Green's function can be readily obtained from Eq. (A2). It has an explicit form

$$\bar{G}^r(\mathbf{r},\mathbf{r}';\omega)=\sum_n \frac{\varphi_n(\mathbf{r})\varphi_n(\mathbf{r}')^*}{s(\omega)-s_n}. \tag{A4}$$

Two features of this expansion are important. First, it separates the dependences on geometry and material properties. The geometrical properties of the nanosystem enter only through the eigenfunctions φ_n and eigenvalues s_n, which are independent of the material properties of the system. Therefore they can be computed for a given geometry once and stored, which simplifies and accelerates further computations. Complementarily, the material properties of the system enter Eq. (A4) only through a single function: spectral parameter s_n.

The second important feature is that this Green's function satisfies exact analytical properties due to the form of Eq. (A4), which contains only simple poles in the lower half-plane of the complex frequency ω and does not have any singularities in the upper half-plane of ω. Consequently, $\bar{G}^r$ is a retarded Green's function that automatically guarantees the causality of the results of time-dependent calculations. Namely, $\bar{G}^r(\mathbf{r},\mathbf{r}';t)=0$ for $t<0$.

Having this Green's function, we can find the local field potential $\varphi(\mathbf{r},\omega)$ generated by the nanosystem in response to any excitation field (external potential) $\varphi_0(\mathbf{r},\omega)$,

$$\varphi(\mathbf{r})=\varphi_0(\mathbf{r},\omega)-\int_V \varphi_0(\mathbf{r}',\omega)\frac{\partial}{\partial\mathbf{r}'}\Theta(\mathbf{r}')\frac{\partial}{\partial\mathbf{r}'}\bar{G}^r(\mathbf{r},\mathbf{r}';\omega)d^3r'. \tag{A5}$$

We can also introduce the retarded tensor Green's function $G^r_{\alpha\beta}$ in terms of the corresponding scalar Green's function $\bar{G}^r$:

$$G^r_{\alpha\beta}(\mathbf{r},\mathbf{r}';\omega)=\frac{\partial^2}{\partial r_\alpha\,\partial r'_\beta}\bar{G}^r(\mathbf{r},\mathbf{r}';\omega), \tag{A6}$$

where $\alpha,\beta=x,y,z$ are vector indices. This tensor determines components of the dyadic in Eq. (2): $(\mathbf{G}^r)_{\alpha\beta}=G^r_{\alpha\beta}(\mathbf{r},\mathbf{r}';\omega)$. For excitation from a far zone, the external field $\mathbf{E}_0$ is uniform, $\varphi_0(\mathbf{r},\omega)=-\mathbf{E}_0(\omega)\mathbf{r}$. Taking this into account and Fourier transforming Eq. (A5) to the time domain, we obtain Eq. (1).

To find the reaction of the system to a source of dielectric polarization $\mathbf{P}(\mathbf{r},t)$, we consider the continuity Eq. (A1) where the right-hand side is changed to $4\pi(\partial\mathbf{P}/\partial\mathbf{r})/\varepsilon_d$. Applying the Green's function to this equation, we obtain the resulting local potential as

$$\varphi^L(\mathbf{r},\omega)=\frac{4\pi}{\varepsilon_d}\int d^3r'\ G^r(\mathbf{r},\mathbf{r}';\omega)\frac{\partial\mathbf{P}(\mathbf{r}',\omega)}{\partial\mathbf{r}'}. \tag{A7}$$

Employing the Gauss theorem (integrating by part), we find the corresponding local field

$$\mathbf{E}^L(\mathbf{r},\omega)=\frac{4\pi}{\varepsilon_d}\int d^3r'\ \mathbf{G}^r(\mathbf{r},\mathbf{r}';\omega)\mathbf{P}(\mathbf{r}',\omega), \tag{A8}$$

where we use the dyadic notations. For a oscillating point dipole $\mathbf{d}(t)$ at a position $\mathbf{r}_0$, we have $\mathbf{P}(\mathbf{r},t)=\delta(\mathbf{r}-\mathbf{r}_0)\mathbf{d}(t)$. Using this to eliminate the integration in Eq. (A8) and transforming it to the time domain, we finally obtain Eq. (2).

*xtli@sjtu.edu.cn
†mstockman@gsu.edu

[1] L. Novotny and B. Hecht, *Principles of Nano-Optics* (Cambridge University Press, Cambridge, England, 2006).
[2] *Topics in Applied Physics*, edited by S. Kawata (Springer Verlag, Berlin, 2001), Vol. 81.
[3] M. I. Stockman, S. V. Faleev, and D. J. Bergman, Phys. Rev. Lett. **87**, 167401 (2001).
[4] M. I. Stockman, M. F. Kling, U. Kleineberg, and F. Krausz, Nat. Photonics **1**, 539 (2007).
[5] T. Klar, M. Perner, S. Grosse, G. von Plessen, W. Spirkl, and J. Feldmann, Phys. Rev. Lett. **80**, 4249 (1998).
[6] J. Lehmann, M. Merschdorf, W. Pfeiffer, A. Thon, S. Voll, and G. Gerber, Phys. Rev. Lett. **85**, 2921 (2000).
[7] J. Bosbach, C. Hendrich, F. Stietz, T. Vartanyan, and F. Trager, Phys. Rev. Lett. **89**, 257404 (2002).
[8] C. Hendrich, J. Bosbach, F. Stietz, F. Hubenthal, T. Vartanyan, and F. Trager, Appl. Phys. B: Lasers Opt. **76**, 869 (2003).
[9] T. Zentgraf, A. Christ, J. Kuhl, and H. Giessen, Phys. Rev. Lett. **93**, 243901 (2004).
[10] M. I. Stockman, Phys. Rev. Lett. **93**, 137404 (2004).
[11] A. Ono, J. I. Kato, and S. Kawata, Phys. Rev. Lett. **95**, 267407 (2005).
[12] G. Shvets, S. Trendafilov, J. B. Pendry, and A. Sarychev, Phys. Rev. Lett. **99**, 053903 (2007).
[13] J. B. Pendry, Opt. Express **11**, 755 (2003).
[14] Z. Liu, H. Lee, Y. Xiong, C. Sun, and X. Zhang, Science **315**, 1686 (2007).
[15] M. I. Stockman, S. V. Faleev, and D. J. Bergman, Phys. Rev. Lett. **88**, 067402 (2002).
[16] D. J. Tannor and S. A. Rice, J. Chem. Phys. **83**, 5013 (1985).
[17] *Principles of the Quantum Control of Molecular Processes*, edited by P. Brumer and M. Shapiro (Wiley, New York, 2003).
[18] R. S. Judson and H. Rabitz, Phys. Rev. Lett. **68**, 1500 (1992).
[19] G. Kurizki, M. Shapiro, and P. Brumer, Phys. Rev. B **39**, 3435 (1989).
[20] T. C. Weinacht, J. Ahn, and P. H. Bucksbaum, Nature (London) **397**, 233 (1999).
[21] P. Brumer and M. Shapiro, Annu. Rev. Phys. Chem. **43**, 257 (1992).
[22] H. Rabitz, R. de Vivie-Riedle, M. Motzkus, and K. Kompa, Science **288**, 824 (2000).
[23] J. M. Geremia and H. Rabitz, Phys. Rev. Lett. **89**, 263902 (2002).
[24] N. A. Nguyen, B. K. Dey, M. Shapiro, and P. Brumer, J. Phys. Chem. A **108**, 7878 (2004).

[25] M. Shapiro and P. Brumer, Phys. Rep. **425**, 195 (2006).
[26] A. Assion, T. Baumert, M. Bergt, T. Brixner, B. Kiefer, V. Seyfried, M. Strehle, and G. Gerber, Science **282**, 919 (1998).
[27] R. Bartels, S. Backus, E. Zeek, L. Misoguti, G. Vdovin, I. P. Christov, M. M. Murnane, and H. C. Kapteyn, Nature (London) **406**, 164 (2000).
[28] N. Dudovich, D. Oron, and Y. Silberberg, Nature (London) **418**, 512 (2002).
[29] T. Brixner, G. Krampert, T. Pfeifer, R. Selle, G. Gerber, M. Wollenhaupt, O. Graefe, C. Horn, D. Liese, and T. Baumert, Phys. Rev. Lett. **92**, 208301 (2004).
[30] M. I. Stockman, D. J. Bergman, and T. Kobayashi, Phys. Rev. B **69**, 054202 (2004).
[31] M. I. Stockman and P. Hewageegana, Nano Lett. **5**, 2325 (2005).
[32] M. Sukharev and T. Seideman, Nano Lett. **6**, 715 (2006).
[33] A. Kubo, K. Onda, H. Petek, Z. Sun, Y. S. Jung, and H. K. Kim, Nano Lett. **5**, 1123 (2005).
[34] M. Aeschlimann, M. Bauer, D. Bayer, T. Brixner, F. J. G. de Abajo, W. Pfeiffer, M. Rohmer, C. Spindler, and F. Steeb, Nature (London) **446**, 301 (2007).
[35] M. Bauer, C. Wiemann, J. Lange, D. Bayer, M. Rohmer, and M. Aeschlimann, Appl. Phys. A: Mater. Sci. Process. **88**, 473 (2007).
[36] A. Derode, A. Tourin, J. de Rosny, M. Tanter, S. Yon, and M. Fink, Phys. Rev. Lett. **90**, 014301 (2003).
[37] G. Lerosey, J. de Rosny, A. Tourin, A. Derode, G. Montaldo, and M. Fink, Phys. Rev. Lett. **92**, 193904 (2004).
[38] G. Lerosey, J. de Rosny, A. Tourin, and M. Fink, Science **315**, 1120 (2007).
[39] P. B. Johnson and R. W. Christy, Phys. Rev. B **6**, 4370 (1972).
[40] M. I. Stockman, in *Surface Enhanced Raman Scattering—Physics and Applications*, edited by K. Kneipp, M. Moskovits, and H. Kneipp (Springer-Verlag, Heidelberg, 2006), pp. 47–66.
[41] M. I. Stockman, L. N. Pandey, L. S. Muratov, and T. F. George, Phys. Rev. B **51**, 185 (1995).
[42] M. I. Stockman, Phys. Rev. Lett. **79**, 4562 (1997).
[43] L. D. Landau and E. M. Lifshitz, *The Classical Theory of Fields* (Pergamon Press, Oxford, 1975).
[44] A. Kubo, N. Pontius, and H. Petek, Nano Lett. **7**, 470 (2007).
[45] E. Verhagen, L. Kuipers, and A. Polman, Nano Lett. **7**, 334 (2007).
[46] L. S. Levitov, Phys. Rev. Lett. **64**, 547 (1990).
[47] D. J. Bergman and D. Stroud, in *Solid State Physics*, edited by H. Ehrenreich and D. Turnbull (Academic Press, Boston, 1992), Vol. 46, pp. 148–270.